Neutral Hydrogen in the Local Universe

D. Obreschkow

Astrophysics, Department of Physics, University of Oxford, Keble Road, Oxford, OX1 3RH, UK

Abstract. We revisit the composition of neutral hydrogen, i.e. atomic (HI) and molecular (H_2), in the local Universe, with focus on the H_2-to-HI mass ratio $\eta_{\rm gal}$ in various galaxies and the H_2-mass function (MF). First, we derive the H_2-MF from the CO-luminosity function (LF) of the FCRAO Extragalactic CO Survey, using a variable CO-to-H_2 conversion fitted to nearby observations. This implies a universal H_2 density $\Omega_{H_2} = (6.9 \pm 2.7) \cdot 10^{-5} h^{-1}$ and $\Omega_{H_2}/\Omega_{\rm HI} = 0.26 \pm 0.11$, which could, however, suffer from incompleteness of the CO-sample. Therefore, a second approach derives the H_2-MF from a HI-sample with well described completeness (HIPASS). This premisses an estimation of $\eta_{\rm gal}$, for which we introduce a set of phenomenological models based on a sample of 245 galaxies drawn from the literature. Our best model in terms of statistical scatter describes $\eta_{\rm gal}$ as a function of galaxy type and cold gas mass. This model leads to an H_2-MF that matches the one derived from the CO-LF, thus supporting that model and settling completeness uncertainties.

Keywords: ISM, Cold gas, Hydrogen, Molecular gas
PACS: 98.58, 67.63, 67.80

1. INTRODUCTION

Neutral hydrogen in galaxies coexists in the atomic (HI) and molecular phase (H_2). Most H_2-mass estimations rely on indirect tracers with uncertain conversion factors. In consequence, the mass ratio $\eta \equiv d{\rm M}_{H_2}/d{\rm M}_{\rm HI}$ and its value for individual galaxies $\eta_{\rm gal} \equiv {\rm M}_{H_2}/{\rm M}_{\rm HI}$ remain uncertain, and estimates of the universal average $\eta_{\rm u} = \Omega_{H_2}/\Omega_{\rm HI}$ vary by an order of magnitude at $z = 0$ (e.g. 0.14 [1], 0.42 [2], 1.1 [3]). This issue culminates in the comparison of simulated cold gas-MFs with observed HI-MFs, as illustrated in Fig. 1 showing various HI-MFs derived from two simulated cold gas-MFs.

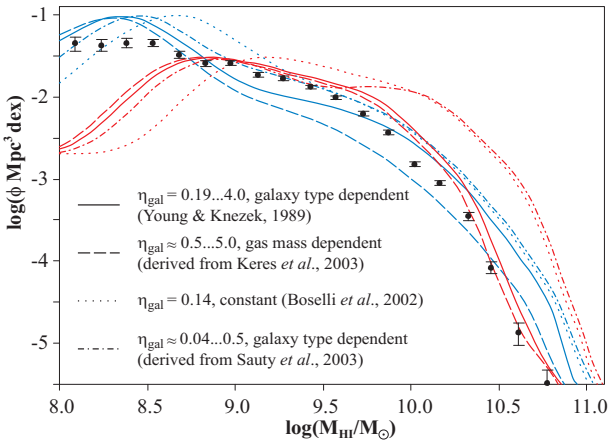

FIGURE 1. Observed HI-MF [6] (points) vs simulated HI-MFs derived from two semi-analytic models [7] (red) and [8] (blue) for recent models of $\eta_{\rm gal}$. All plots adopt $H_0 = 73\,{\rm km\,s^{-1}\,Mpc^{-1}}$.

This proceeding aims at unifying recent studies of the HI-MF, CO-LF, CO-to-H_2 conversion (X-factor), and $\eta_{\rm gal}$ in various galaxies. In Sect. 2, we recover the *H_2-MF from the CO-LF* [2]. Uncertainties caused by the incompleteness of the underlying sample are bypassed in Sect. 3, where we construct the *H_2-MF from the HIPASS HI-sample* with well characterized completeness. As this approach premisses a model of $\eta_{\rm gal}$, which itself relies on H_2-estimations from CO, both approaches ultimately depend on the X-factor, for which we use a galaxy dependent model.

2. H_2-MF FROM CO DATA

2.1. CO-to-H_2 Conversion Revisited

Most H_2-mass estimations rely on indirect detections of the CO-rotation line at 115 GHz, which is powered by H_2-CO collisions and hence dependent on the H_2-mass $\mathrm{M_{H_2}}$, the ratio $\mathrm{M_{H_2}/M_{CO}}$, and pressure. CO is optically thick for this radiation; thus the 115 GHz rest frame luminosity L_{115} is a non-linear mass tracer for individual clouds. However, detailed studies revealed that on kiloparsec scales (hundreds of clouds) CO is effectively thin [9, 10], in the sense that L_{115} is nearly proportional to $\mathrm{M_{H_2}}$, or more precisely [11],

$$\frac{\mathrm{M_{H_2}}}{\mathrm{M_\odot}} = 5.37\cdot 10^3 \cdot X \cdot \frac{S_{115}}{\mathrm{Jy\,km\,s^{-1}}} \cdot \left(\frac{D_l}{\mathrm{Mpc}}\right)^2 = 1.17\cdot 10^{-22}\cdot X \cdot \frac{L_{115}}{W} \qquad (1)$$

where S_{115} is the integrated line flux and D_l is the luminosity distance. In this equation, the dimensionless ratio $X \equiv [N(\mathrm{H_2})/\mathrm{cm^{-2}}]/[I_{115}/(\mathrm{K\,km\,s^{-1}})]\cdot 10^{-20}$ is assumed constant for identical average cloud properties (geometry, metallicity, pressure).

The observational determination of X requires CO-independent H_2-measurements, which are currently restricted to a few nearby galaxies. Typical methods use the virial-mass of giant molecular clouds [12], the line ratios of different CO isotopes [13], the gas-to-dust ratio [14, 15], or γ-ray data [16]. Based on early findings that X is constant in the inner $2-10$ kpc of the Galaxy, several authors (e.g. [12]) concluded that X does not depend on average cloud properties. This assertion was later rejected [17, 1], when larger samples pinpointed a clear correlation between X and the average metallicity.

We use a variable X-factor X_ν depending on the extinction corrected absolute blue magnitude $M_{\rm B}$ or the rest frame 115 GHz-luminosity L_{115}. These relations are almost as tight as the metallicity-dependent one, and we prefer them for the widespread availability of $M_{\rm B}$-data and the implicit access to L_{115}. The observational data (Fig. 2, left) was drawn from the literature and the best linear fit minimizing the square deviations while respecting the relation between L_{115} and $M_{\rm B}$ (based on the 245 galaxies in § 3.1) is,

$$\log(X_\nu) = 8.63 - 0.309\,\log(L_{115}\,h^2\mathrm{W^{-1}}) \pm \sigma_X = 3.35 + 0.159\,(M_{\rm B} - 5\log h) \pm \sigma_X \quad (2)$$

Both relations have the same rms-scatter of 0.29 in $\log(X)$, which implies a physical scatter of $\sigma_X = 0.26$ when accounting for the observational noise of 0.13 dex. To compare the following results to the ones obtained with a constant X-factor, we will also use a constant model $\log(X_c) = \log(2) \pm \sigma_X$ [25] with the same scatter.

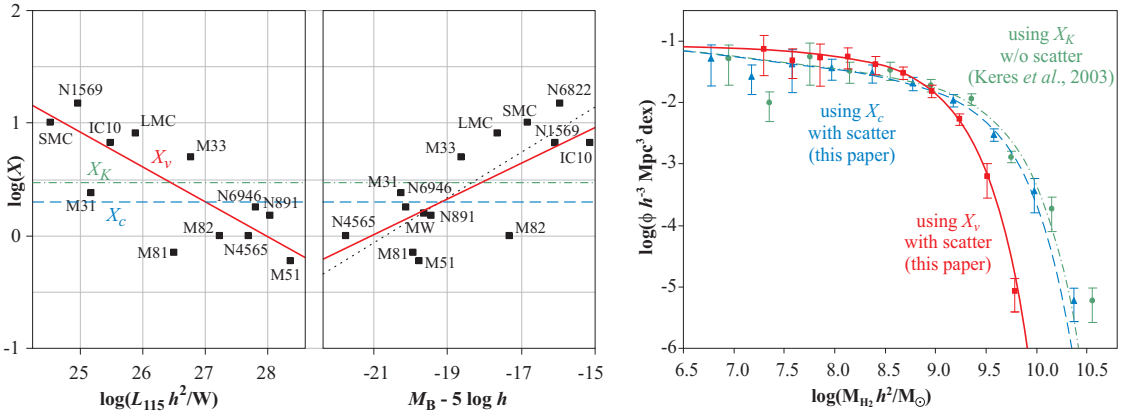

FIGURE 2. LEFT: (Points) Measured X-factor as a function of 115 GHz luminosity L_{115} and absolute blue magnitude M_B for 14 local galaxies [1, 18, 1, 19, 20, 21, 22, 23, 24], (red solid lines) our best variable model X_v, (blue dashed lines) our constant choice X_c, (green dash-dotted lines) constant choice by [2], (dotted line) fit by [1]. RIGHT: H_2-MFs derived from the CO-LF presented by [2], using the three models for the X-factor shown on the left; X_v and X_c were applied with scatter, X_K without scatter.

TABLE 1. Schechter parameters and implied densities. η_u uses $\Omega_{HI} = (2.6 \pm 0.3) \cdot 10^{-4}\, h^{-1}$ [6].

	$\frac{M^*}{10^9\, h^{-2}\, M_\odot}$	α	$\frac{\theta}{h^3\, \mathrm{Mpc}^{-3}\, \mathrm{dex}^{-1}}$	Red. χ^2	$\frac{\rho_{H_2}}{10^7\, h\, M_\odot\, \mathrm{Mpc}^{-3}}$	$\frac{\Omega_{H_2}}{10^{-4}\, h^{-1}}$	η_u
X_c	2.43	-1.20	0.0082	0.34	2.3 ± 0.9	0.83 ± 0.31	0.32 ± 0.13
X_v	**0.75**	$\mathbf{-1.07}$	**0.0243**	**0.05**	$\mathbf{1.9 \pm 0.7}$	$\mathbf{0.69 \pm 0.27}$	$\mathbf{0.26 \pm 0.11}$
X_K	2.81	-1.18	0.0089	2.55	2.8 ± 1.1	1.0 ± 0.39	0.39 ± 0.16

2.2. H_2-MF from CO-LF

We shall now extract H_2-MFs from the CO-LF presented by [2]. The latter is based on a far infrared-selected subsample (200 galaxies) of the FCRAO Extragalactic CO Survey [26], which successfully reproduced the 60μm-LF, despite its poorly understood completeness. We first converted the luminosity units used in [2] to Watts (1 Jy km s^{-1} Mpc^2 is $3.65 \cdot 10^{24}$ W at 115 GHz) and then transformed the CO-LF to a H_2-MF via relation (1), right. For the X-factor we used the two models introduced above (i.e. the constant value X_c and the variable value X_v, both with scatter) and the constant value $X_K = 3$ without scatter used by [2] to derive the first H_2-MF.

The resulting H_2-MFs are displayed in Fig. 2 together with the Schechter functions minimizing the weighted square deviations. Function parameters and resulting gas densities are listed in Table 1. For the constant X-factor, the change from the H_2-MF by [2] to our model is small, the total density ρ_{H_2} decreasing by about 19%. This is the combined effect of a mass-shift $X_c/X_K = 0.67$ and the addition of scatter, which slightly raises the high-mass end, thus reincreasing ρ_{H_2} by a factor 1.22. However, our variable X-factor significantly compresses the MF and ρ_{H_2} drops by 33%. In this preferred H_2-MF, the global H_2-to-HI ratio equals $26 \pm 11\%$, implying a cold gas density $\Omega_g = (4.5 \pm 0.8) \cdot 10^{-4}\, h^{-1}$ composed of $59 \pm 6\%$ HI, $15 \pm 6\%$ H_2, 24% Helium, 2% Metals (uncertainties of HI and H_2 are anti-correlated).

3. H_2-MF FROM COMBINED HI+CO DATA

In this section, we derive *phenomenological* models for the galaxy-averaged molecular ratio $\eta_{\rm gal}$. All models will be applied to recover H_2-MFs from the complete HI-data in HIPASS, thus providing an alternative to using the CO-LF.

3.1. Molecular-to-Atomic Gas in Different Galaxies

Our sample of 245 distinct galaxies (presented in [27]) was drawn from the literature [28, 29, 30, 5, 31, 32, 23, 33, 34, 4, 18] and includes homogenized CO-line fluxes, HI-masses, galaxy types T, and extinction corrected absolute B-band magnitudes $M_{\rm B}$. The latter served to determine the variable X-factor X_ν (eq. 2), used to convert CO-fluxes in H_2-masses (eq. 1). (We chose to evaluate X_ν from $M_{\rm B}$ rather than L_{115} because most galaxies in the sample exhibit more accurate measurements of $M_{\rm B}$.) Our sample covers a wide range of galaxy types, masses, and environments, and has 49% overlap with the subsample of the FCRAO Extragalactic CO Survey used for the CO-LF by Keres et al. (see prev. Sect.). We deliberately limited the overlap of the two samples to 50%, in order to control sample biases.

This sample exhibits clear correlations found between $\eta_{\rm gal}$ and T and cold gas mass $\mathrm{M_g}$, and we shall introduce three models based on these correlations. Model 1 is galaxy type dependent, as suggested by Fig. 3 (left) and earlier studies [e.g. 4, 5]. The ratio $\eta_{\rm gal}$ increases by roughly an order of magnitude when passing from late-type spirals (Scd-Sd) to early-type spirals and lenticulars (S0-S0/a) – a trend that can be explained by the higher gas pressure in the bulge component [27]. The monotonous trend seems to break down between lenticular and elliptical galaxies, where the physical situation becomes more complex. In fact, many ellipticals comprise molecular gas in their center with no detectable HI-counterpart (e.g. Virgo cluster ellipticals), while others exhibit HI-dominated outer regions left over by mergers. To tackle the different behavior of ellipticals and spirals we chose a piecewise linear relation with different parameters for the two populations,

$$\log(\eta_{\rm gal,1}) = \left\{ \begin{array}{ll} c_0^{el} + c_1^{el}\,T & \text{if } T < T_0 \\ c_0^{sp} + c_1^{sp}\,T & \text{if } T \geq T_0 \end{array} \right\} + \sigma_{\rm phy} \qquad (3)$$

where c_0^{el}, c_1^{el}, c_0^{sp}, c_1^{sp} are free parameters to be fitted to the data, and T_0 is at the intersection of the two straight lines, i.e. $c_0^{el} + c_1^{el}\,T_0 \equiv c_0^{sp} + c_1^{sp}\,T_0$. $\sigma_{\rm phy}$ denotes an estimation of the true physical scatter.

Model 2 addresses the correlation between $\eta_{\rm gal}$ and $\mathrm{M_g}$. Motivated by the roughly linear correlation in our sample, we chose the form

$$\log(\eta_{\rm gal,2}) = k_0 + k_1\,\log(\mathfrak{m}_{\rm g}) + \sigma_{\rm phy} \qquad (4)$$

where $\mathfrak{m}_{\rm g} \equiv \mathrm{M_g}/[10^9\,h^{-2}\,\mathrm{M_\odot}]$, and k_0, k_1 are free parameters.

In principle, the type-dependent model 1 and the cold gas mass-dependent model 2 could be different manifestations of the same relation, if they are related via a type-dependence of the average cold gas mass. To lift a possible degeneracy, and because

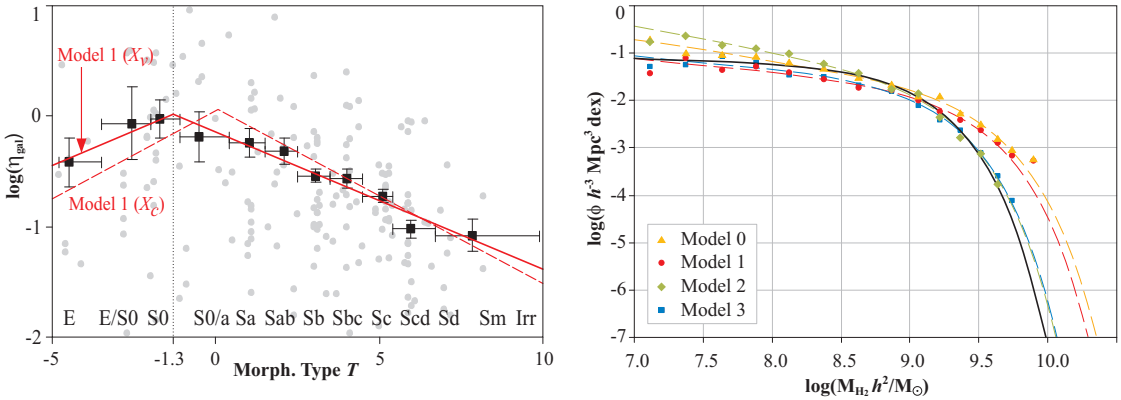

FIGURE 3. LEFT: Mass ratio versus numerical Hubble type. (dots) data points obtained via the variable factor X_v with scatter; (black points) binned data, vertical bars are statistical uncertainties obtained via bootstrapping, horizontal bars are the bin intervals; (solid line) model 1 fitted to the data points [not to the bins]; (dashed line) model 1 fitted to the undisplayed data points for the constant factor X_c. RIGHT: (various symbols) H_2-MFs constructed from the HIPASS HI-catalog using the different HI-to-H_2 conversion models derived in § 3.1, (dashed lines) Schechter fits, (black solid line) Schechter function matching the H_2-MF derived from the CO-LF, also shown in Fig. 2 (right). All functions correspond to models with variable conversion X_v.

a simultaneous dependence on two galaxy properties is suggested by the analytical derivation in [27], we shall introduce the bilinear model 3,

$$\log(\eta_{\rm gal,3}) = \left\{ \begin{array}{l} c_0^{el} + c_1^{el}\, T\ (< T_0) \\ c_0^{sp} + c_1^{sp}\, T\ (\geq T_0) \end{array} \right\} + k_1 \log(\mathrm{M_g}) + \sigma_{\rm phy} \qquad (5)$$

where c_0^{el}, c_1^{el}, c_0^{sp}, c_1^{sp}, k_1 are free parameters and $c_0^{el} + c_1^{el}\, T_0 \equiv c_0^{sp} + c_1^{sp}\, T_0$.

To compare the three models with a constant molecular fraction, such as often used in the literature, we finally introduce a constant model 0, $\log(\eta_{\rm gal,0}) = c_0 + \sigma_{\rm phy}$.

The free parameters were determined by minimizing the rms-deviation of $\log(\eta_{\rm gal})$ from the model predictions. Optimization in log-space is the only reasonable choice, since $\eta_{\rm gal}$ is subject to Gaussian scatter in log-space. Therefore, only models fitted in log-space can be ascribed simple Gaussian scatter, whereas other fits require more complex distributions. The most probable values and likelihoods of all parameters are summarized in Table 2 for both conversion factors X_v and X_c. Our estimation of the true physical scatters $\sigma_{\rm phy}$ is explained in [27], but we already note that the generally smaller scatter in case of a variable conversion factor X_v supports the variable H_2-CO conversion against a constant one.

3.2. Recovering the H_2-MF from HI-data

Applying the above models of $\eta_{\rm gal}$, we recovered the H_2-MF from the HI-data in the HIPASS catalog (see Fig. 3, right). For comparison, the plot also includes the H_2-MF derived from the CO-LF using the same conversion factor (black solid line). Clearly, model 3 provides the best simultaneous agreement for small and high masses. Model 1

TABLE 2. Most likely parameters for the four models of $\eta_{\rm gal}$.

	variable X_v		**constant X_c**	
0	$c_0 = -0.58^{+0.16}_{-0.23}$	$\sigma_{\rm phy} = 0.39$	$c_0 = -0.50^{+0.16}_{-0.23}$	$\sigma_{\rm phy} = 0.44$
1	$c_0^{el} = +0.18^{+0.40}_{-0.22}$ $c_1^{el} = +0.12^{+0.14}_{-0.05}$ $T_0 = -1.3^{+1.2}_{-0.5}$)	$c_0^{sp} = -0.14^{+0.10}_{-0.07}$ $c_1^{sp} = -0.12^{+0.01}_{-0.02}$ $\sigma_{\rm phy} = 0.27$	$c_0^{el} = +0.06^{+0.28}_{-0.12}$ $c_1^{el} = +0.16^{+0.07}_{-0.04}$ $T_0 = 0.0^{+0.4}_{-0.4}$	$c_0^{sp} = +0.07^{+0.11}_{-0.17}$ $c_1^{sp} = -0.16^{+0.03}_{-0.03}$ $\sigma_{\rm phy} = 0.33$
2	$k_0 = -0.51^{+0.03}_{-0.04}$ $k_1 = -0.24^{+0.05}_{-0.05}$	$\sigma_{\rm phy} = 0.30$	$k_0 = -0.53^{+0.03}_{-0.04}$ $k_1 = 0.00^{+0.05}_{-0.07}$	$\sigma_{\rm phy} = 0.42$
3	$c_0^{el} = -0.01^{+0.25}_{-0.16}$ $c_1^{sp} = -0.13^{+0.02}_{-0.02}$ $k_1 = -0.18^{+0.06}_{-0.07}$ $\sigma_{\rm phy} = 0.15$	$c_0^{sp} = -0.02^{+0.10}_{-0.09}$ $c_1^{el} = +0.13^{+0.07}_{-0.04}$ $T_0 = -0.1^{+1.2}_{-0.6}$	$c_0^{el} = +0.05^{+0.26}_{-0.21}$ $c_1^{el} = +0.14^{+0.11}_{-0.05}$ $k_1 = +0.06^{+0.11}_{-0.11}$ $\sigma_{\rm phy} = 0.33$	$c_0^{sp} = +0.05^{+0.10}_{-0.21}$ $c_1^{sp} = -0.16^{+0.02}_{-0.03}$ $T_0 = -0.0^{+1.5}_{-0.5}$

over-estimates the density of heavy H_2-masses, probably by over-estimating $\eta_{\rm gal}$ of gas-richest early-type spiral galaxies. The latter have a low molecular fraction (see model 2), but they are a minority within otherwise gas-poor but molecule-rich early-type spirals. While model 2 overcomes this issue and produces the right density of heavy H_2-masses, it fails by a factor 3-4 in the low-mass end ($M_{H_2} \lesssim 10^8 M_\odot$). This is a direct manifestation of assigning high molecular fractions to all gas-poor galaxies, which neglects small young spirals with a dominant atomic phase. Finally, model 0 seems to suffer from similar limitations in both ends of the H_2-MF.

The *increasing* mutual agreement between the CO-LF-based H_2-MF and HI-based H_2-MFs with increasing model complexity is an indicator for the good quality of the H_2-MF derived from the CO-LF. With regard to the unknown completeness, Keres et al. [2] confirmingly argued that their CO-LF does not substantially suffer from incompleteness by analyzing the FIR-LF produced from the same sample. The surprisingly strong *agreement of model 3 in particular* supports this mass- and type-dependent model against models depending on one parameter only. This affirmation will be strongly supported by our analytical derivation of $\eta_{\rm gal}$ in [27].

4. OUTLOOK

A detailed analysis of the ratio $\eta_{\rm gal}$ is presented in forthcoming papers. This will include

- Discussion of the scatter of our phenomenological models of $\eta_{\rm gal}$.
- Analytical derivation of the $\eta_{\rm gal}$ based on the η-pressure relation [35].
- Local cold gas-MF (HI+H_2+He) derived from the HIPASS data using our best model of $\eta_{\rm gal}$.
- HI and H_2 in cosmological simulations: application of our best model of $\eta_{\rm gal}$ to simulate HI- and CO-emission lines based on simulated galaxy catalogs.
- Extended discussion of the cosmological evolution of $\eta_{\rm gal}$, $\Omega_{\rm HI}$ and Ω_{H_2}.

REFERENCES

1. A. Boselli, J. Lequeux, and G. Gavazzi, *Astron. Astrophys.* **384**, 33–47 (2002), arXiv:astro-ph/0112275.
2. D. Keres, M. S. Yun, and J. S. Young, *Astrophys J.* **582**, 659–667 (2003), arXiv:astro-ph/0209413.
3. M. Fukugita, C. J. Hogan, and P. J. E. Peebles, *Astrophys J.* **503**, 518–+ (1998), arXiv:astro-ph/9712020.
4. J. S. Young, and P. M. Knezek, *Astrophys J. Lett.* **347**, L55–L58 (1989).
5. S. Sauty, F. Casoli, A. Boselli, M. Gerin, J. Lequeux, J. Braine, G. Gavazzi, J. Dickey, I. Kazès, and P. Fouqué, *Astron. Astrophys.* **411**, 381–390 (2003).
6. M. A. Zwaan, M. J. Meyer, L. Staveley-Smith, and R. L. Webster, *Mon. Not. R. Astron. Soc.* **359**, L30–L34 (2005), arXiv:astro-ph/0502257.
7. R. G. Bower, A. J. Benson, R. Malbon, J. C. Helly, C. S. Frenk, C. M. Baugh, S. Cole, and C. G. Lacey, *Mon. Not. R. Astron. Soc.* **370**, 645–655 (2006), arXiv:astro-ph/0511338.
8. G. De Lucia, and J. Blaizot, *Mon. Not. R. Astron. Soc.* **375**, 2–14 (2007), arXiv:astro-ph/0606519.
9. K. M. Ferrière, *Reviews of Modern Physics* **73**, 1031–1066 (2001), arXiv:astro-ph/0106359.
10. W. F. Wall, *Revista Mexicana de Astronomia y Astrofisica* **42**, 117–126 (2006).
11. C. D. Wilson, and N. Scoville, *Astrophys J.* **363**, 435–450 (1990).
12. J. S. Young, and N. Z. Scoville, *Annu. Rev. Astron. Astrophys.* **29**, 581–625 (1991).
13. W. Wild, A. I. Harris, A. Eckart, R. Genzel, U. U. Graf, J. M. Jackson, A. P. G. Russell, and J. Stutzki, *Astron. Astrophys.* **265**, 447–464 (1992).
14. M. Guelin, R. Zylka, P. G. Mezger, C. G. T. Haslam, E. Kreysa, R. Lemke, and A. W. Sievers, *Astron. Astrophys.* **279**, L37–L40 (1993).
15. M. Guelin, R. Zylka, P. G. Mezger, C. G. T. Haslam, and E. Kreysa, *Astron. Astrophys.* **298**, L29+ (1995).
16. S. D. Hunter, D. L. Bertsch, J. R. Catelli, T. M. Dame, S. W. Digel, B. L. Dingus, J. A. Esposito, C. E. Fichtel, R. C. Hartman, G. Kanbach, D. A. Kniffen, Y. C. Lin, H. A. Mayer-Hasselwander, P. F. Michelson, C. von Montigny, R. Mukherjee, P. L. Nolan, E. Schneid, P. Sreekumar, P. Thaddeus, and D. J. Thompson, *Astrophys J.* **481**, 205–+ (1997).
17. N. Arimoto, Y. Sofue, and T. Tsujimoto, *Pub. Astron. Soc. Japan* **48**, 275–284 (1996).
18. G. Paturel, C. Petit, P. Prugniel, G. Theureau, J. Rousseau, M. Brouty, P. Dubois, and L. Cambrésy, *Astron. Astrophys.* **412**, 45–55 (2003).
19. M. Rubio, G. Garay, J. Montani, and P. Thaddeus, *Astrophys J.* **368**, 173–177 (1991).
20. J. S. Young, S. Xie, J. D. P. Kenney, and W. L. Rice, *Astrophys J. Suppl.* **70**, 699–722 (1989).
21. M. H. Heyer, T. M. Dame, and P. Thaddeus, "The molecular gas component of M31 and the Milky Way," in *Proceedings 232. WE-Heraeus Seminar*, edited by E. M. Berkhuijsen, R. Beck, and R. A. M. Walterbos, 2000, pp. 29–36.
22. A. Leroy, A. Bolatto, F. Walter, and L. Blitz, *Astrophys J.* **643**, 825–843 (2006), arXiv:astro-ph/0602056.
23. L. J. Sage, *Astron. Astrophys.* **272**, 123–+ (1993).
24. M. H. Heyer, E. Corbelli, S. E. Schneider, and J. S. Young, *Astrophys J.* **602**, 723–729 (2004), arXiv:astro-ph/0311226.
25. T. M. Dame, D. Hartmann, and P. Thaddeus, *Astrophys J.* **547**, 792–813 (2001), arXiv:astro-ph/0009217.
26. J. S. Young, S. Xie, L. Tacconi, P. Knezek, P. Viscuso, L. Tacconi-Garman, N. Scoville, S. Schneider, F. P. Schloerb, S. Lord, A. Lesser, J. Kenney, Y.-L. Huang, N. Devereux, M. Claussen, J. Case, J. Carpenter, M. Berry, and L. Allen, *Astrophys J. Suppl.* **98**, 219–+ (1995).
27. D. Obreschkow et al., (forthcoming) (2008).
28. G. A. Welch, and L. J. Sage, *Astrophys J.* **584**, 260–277 (2003), arXiv:astro-ph/0210337.
29. L. J. Sage, and G. A. Welch, *Astrophys J.* **644**, 850–861 (2006).
30. L. D. Matthews, Y. Gao, J. M. Uson, and F. Combes, *Astron. J.* **129**, 1849–1862 (2005), arXiv:astro-ph/0501359.
31. A. Georgakakis, A. M. Hopkins, A. Caulton, T. Wiklind, A. I. Terlevich, and D. A. Forbes, *Mon. Not. R. Astron. Soc.* **326**, 1431–1440 (2001), arXiv:astro-ph/0105435.

32. P. Andreani, F. Casoli, and M. Gerin, *Astron. Astrophys.* **300**, 43–+ (1995), arXiv:astro-ph/9501014.
33. J. F. Lees, G. R. Knapp, M. P. Rupen, and T. G. Phillips, *Astrophys J.* **379**, 177–215 (1991).
34. H. A. Thronson, Jr., L. Tacconi, J. Kenney, M. A. Greenhouse, M. Margulis, L. Tacconi-Garman, and J. S. Young, *Astrophys J.* **344**, 747–762 (1989).
35. L. Blitz, and E. Rosolowsky, *Astrophys J.* **650**, 933–944 (2006), arXiv:astro-ph/0605035.